Chapter 5

ATC ASSESSMENT AND ENHANCEMENT OF INTEGRATED TRANSMISSION AND DISTRIBUTION SYSTEM CONSIDERING THE IMPACT OF ACTIVE DISTRIBUTION NETWORK

Assessment and enhancement of transmission network capability have been among the prime interests of power system monitoring, operation, and control. Conventionally, the available transfer capability (ATC) assessment has been tackled considering the transmission and distribution networks as segregated entities because they had little or no influence on each other's performance due to the unidirectional flow of power from the transmission to distribution networks. Now, with increasing interest in smart transmission and distribution in amalgamation with a paradigm shift in sources of generation from centralized to decentralized even at distribution levels mandating the analysis of power grid while considering both the hierarchies simultaneously. In this chapter, a platform for the quasi-static operation of power transmission and distribution networks, employing a multi-agent-based system, has been developed. The developed multi-agent system based approach has been utilized to assess ATC considering active distribution network (ADN) whereby Modified IEEE 24 BUS RTS system at transmission and Modified IEEE 123 node system at distribution level has been considered as test systems. It has been observed that the presence of ADN considerably affects the ATC of the system.

5.1 INTRODUCTION

In the evolving scenario of power system restructuring, the assessment and enhancement of power transferring and handling capability of the power network would be playing a very vital role. ATC (available transfer capability) assessment and

enhancement has been an essential aspect of power system operation monitoring and control. The power system is being drastically restructured at transmission, distribution, and generation levels. Conventionally, there used to be unidirectional power flow directed from the source node (i.e., power system substations) to the feeder/consumer end in distribution networks. This facilitated separate analysis of transmission and distribution systems due to the negligible influence of the distribution network on the transmission system. An increase in decentralized and distributed generation increases the complexity and interdependency (in terms of impact) of the transmission and distribution system. The occurrence of reverse power flows in distribution systems on account of increased distributed generation with the dominance of intermittent renewable sources and mobile virtual power plants capable of acting as sink or source depending on the market scenario (electric vehicles) further aggravated the issue by adding to the interdependency of T&D (integrated transmission & distribution) systems. The existing literature on ATC estimation covers in great detail the conventional systems, but little work is done while considering the presence of an Active Distribution Network (ADN). The problem of ATC assessment for integrated T&D system lies with lack of proper method/technique to deal with the complicacy arising because of considering the ADN. Therefore, this chapter first attempts to develop a MAS (multi-agent system) based system for the integrated analysis of the $T\&D$ system and provides a pattern search optimization-based solution for ATC assessment.

Co-simulation platforms for integrated analysis of T&D systems are being developed for assessing the impacts of the probable phenomenon at DN on TN and vice-versa. This chapter, furthering the research, proposes an ITD framework that involves software in loop simulation whereby a multi-agent-based system (MAS) has been used for data exchange between the $T\&D$ at the boundaries for integrated analysis of $T\&D$ and pattern

search-based method for assessment of ATC. Although in the existing literature methods for coordinated optimization of $T\&D$ systems, co-dynamic simulation, and application of the developed framework to different applications can be found, the technique for efficient quasi-static analysis over a larger span along with ATC assessment in the integrated framework is still under development. The main contributions of the chapter are as follows:

- MAS driven approach has been proposed for ITD development and implementation using $MATPOWER$ and $OPENDSS$ co-simulation based models.
- A coordinated scheme using MAS for the ITD framework has been developed to assess the impact of ADN on the ATC of the system at the transmission level.
- The impact of deploying CVR in ADN at DN on the ATC of the system at TN has been analyzed.
- Impact presence and absence of $DERS$ (PV, WIND, PV & WIND) in ADN at DN on ATC of the system at TN has been analyzed.

5.2 ITD FRAMEWORK

The developed framework for integrated analysis of transmission and distribution system ($ITD_{platform}$) is schematically represented in Figure 5.1. The ITD platform relies on agent-based communication between the TSO and DSO. The method is implemented by dividing the system into two levels. The TSO performs the transmission system analysis, control, and monitoring function while being in continuous coordination with the energy management system (EMS). Analogously the DSO performs the functions of the distribution system and is in continuous coordination with the $Advance\ Distribution\ Management\ Server$ (ADMS). That regularly monitors measurements with the help of supervisory control and data acquisition system and AMI

(advanced metering infrastructure). The first step towards establishing the ITD interaction begins with the identification of nodes/buses/substations acting as PCC (Point of Common Coupling) for the T&D interface. Defining the cardinality of such nodes would lead to identifying the size of agents required for facilitating the ITD interaction.

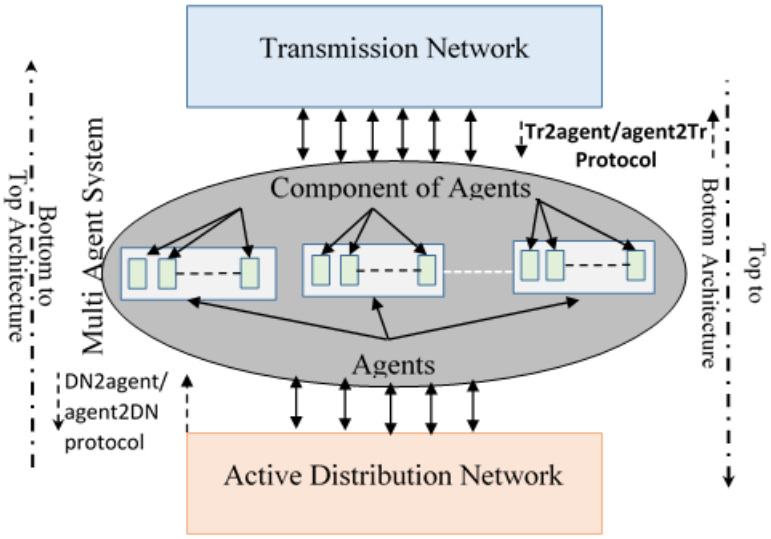

Figure 5.1 Integrated Transmission and Distribution Framework.

5.2.1.1 *pcc Node*

The *pcc* node can be defined as a floating bus. It can be considered as a floating bus because there happens to be a range of operating points at which the states of the *pcc* node may exist [95]. Once the states of the floating bus are obtained, it can be set as PV or PQ bus depending upon the conditions prevailing in the network.

5.2.1.2 *Multi-agent based system*

A multi-agent-based system has been developed to materialize the interaction between the T&D. The architecture of the MAS system has been shown in Figure 5.1. The step-by-step implementation algorithm of MAS has been given in Table 5.1. The MAS consists of several agents α which are employed for exchanging the information between the DSO and the TNO. The proposed MAS system can function in two different modes:

- $Top\ to\ Bottom$ mode: Here, the TN is solved first and then after the states of the PCC are communicated to the ADN where DSO solves the ADN.
- $Bottom\ to\ Top$ mode: In this mode of operation, DSO solves the ADN depending upon the scenarios prevalent in the DN, and states of the ADN are communicated via the agents to the PCC.

The number of agents in the MAS would be equal to the number of ADN's (i.e., the number of PCC) considered. The agent α_j^i represents the jth state of i^{th} agent. Each agent has two major components TSO agent vector and the DSO agent vector. Depending upon the architecture deployed for analysis, these vectors would be determinantal for TSO or DSO side variables

$$\alpha = \{\alpha_1, \alpha_2 \dots, \alpha_{na}\}$$
$$\alpha_i = \{\alpha_i^1, \alpha_i^2, \dots \alpha_i^{na_i}\} \quad 5.1$$

$$agent(\alpha) \Rightarrow agentware(TN, agent, mode)$$
$$agentware|_1 \Rightarrow agent = tr2agent(TN) \forall t2b \quad dn2agent(DN) \forall b2t \quad 5.2$$

$$agentware|_2 \Rightarrow agent = agent2tr(TN, agent)\ \forall\ t2b \quad agent2dn(DN, agent)\ \forall\ b2t \quad 5.3$$

Here, na is the number of agents, na_i is the number of components of i^{th} agent. In $agentware|_{mode}$, $agentware$ is a function containing two subscripts having the protocols of information exchange for TN/DN to the agent and vice-versa, the $mode$ (1 or 2) indicates whether $tr2agent$ (mode 1) or $agent2tr$ (mode 2) in case of top to bottom $(t2b)$ and $dn2agent$ (mode 1) or $agent2dn$ (mode 2) in case of the bottom to top $(b2t)$ architecture would be invoked. The input parameters for $agentware$ are transmission network information (TN), agent (initially a set of null matrices), mode. The

agent α_i contains the information pertinent to the TN node i, P & Q flexibility region of i^{th} interface, state variables at the ith interface in the purview of ADN.

5.2.1.3 *Interface architecture*

The ITD interface can be achieved by using any of the two different architectural typologies, namely, top-to-bottom and bottom-to-top topology. In the bottom-to-top topology, the ADN demands and $DERs$ drive the interface parameters through the DSO, while in the top to bottom architecture, the interface parameters are governed TNO through the TSO. The flexibility of controlling the ADN resources either by dispatching controls from TSO or DSO through a coordinated mechanism could be enabled for enhancing the functioning of the overall system.

5.3 MODELING OF ITD & DER

ATC assessment and enhancement would be affected by the uncertainties in power produced by the $DER'S$. ATC has been conventionally evaluated while considering the predicted/ forecasted value of the demand/generation. When the $DER's$ are taken into consideration, the degree of uncertainty increases substantially; this would adversely affect the ATC assessment. Thus, appropriate models of $DER's$ should be considered while evaluating the ATC. Further, the ATC enhancement could be achieved by utilizing the FACTS devices; therefore, this section presents the model of DER's and FACTS devices which have been used in this work.

5.3.1.1 *Solar PV & smart inverter modeling*

The Solar PV has been modeled as a PQ load where P will be negative for the generation (i.e., injection to the grid), and Q would be positive or negative depending upon the operating conditions of the smart inverter through which the PV is connected.

Uncertainties in PV power output are considered using the β distribution; it has been taken to realize the probability density function of solar irradiance for each hour [160]. The active and reactive power support available from the smart inverter [136] sourced by the PV module is determined by the following equations:

$$P^{inv} = P - P^{inv}_{losses} \tag{5.4}$$

$$Q^{inv} \cong Q \tag{5.5}$$

$$P^{inv}_{losses} = (1 - \eta_{inv}) \times \sqrt{P^2 + Q^2} \tag{5.6}$$

The maximum value of Q^{inv}_{max} is a function of real power generation and is determined by (5.7)

$$\left|Q^{inv}_{max}\right| = \sqrt{S^2_{max} - P^2} \tag{5.7}$$

5.3.1.2 *Wind modeling*

A synthetic wind power model developed from the data measured directly in the wind power domain is used for modeling the uncertainties of power generated from the wind farms [97]. The model uses the Markov Chain Monte Carlo method for generating the time series samples for which the analysis is done. The static wind power characteristics of the wind turbines are typically non-linear, and the relation between the wind speed v and power output is mathematically given by

$$P_w(v) = \begin{cases} 0 & v < v_{ci} \; or \; v > v_{co} \\ P_{w_N} & v_N \le v \le v_{co} \\ f_w(v) & v_{ci} < v \le v_N \end{cases} \tag{5.8}$$

The wind turbine characteristics within the range v_{ci} to v_{co} has been modeled by linearising the non-linear curvature portion of the turbine characteristics; here, nominal power output and function expressing output of wind power in terms of wind speed are P_{w_N} and $f_w(v)$, respectively. The linearization has been done in the following manner:

1. Identify the point at which there is an abrupt change in slope in terms of a, b, n (a_i and b_i being starting and endpoints of the i^{th} slope ranging from 1 to $(n + 1)$, n is the number of abrupt change).
2. Divide the characteristic into $n + 1$ different zones.
3. Linearly model each zone in the form of $y = m * x + c$ ($\forall m, c \in$ constant; $x \in$ independent variable and $y \in$ dependent variable)

$$\begin{aligned} m(i) &= (P_w(b_i) - P(a_i))/(v(b_i) - v(a_i)) \\ c(i) &= P_w(a_i) - m(i) \times v(a_i) \\ y &= P_w(v) \end{aligned} \quad 5.9$$

The model fitted has an MSE (mean squared error) of 0.023. The MSE for the fitted model can be increased by increasing the number of regions in which the non-linear curve is broken for modeling the characteristic.

5.3.1.3 *Modeling of FACTS*

The power flow through the lines could be controlled by controlling the parameters of the FACTS devices. The modeling of the FACTS devices, namely SVC and $TCSC$ that have been considered in this chapter, has been discussed in Chapter 2 section 2.5.1.

5.3.1.4 *ITD modeling*

The transmission and distribution system has been modeled by identifying the nodes at which the active distribution system is considered as a PCC (point of common coupling). The ADN has been represented by a combination of several DN feeders.

$$ADN_{load} = \pi Pd^{DN} \quad 5.10$$

$$Fixed_{load}^{pcc} = Pd_i^{pcc} - \tau Pd^{DN} \quad 5.11$$

$$\%ADN_{load} = \frac{\sum_{i=1}^{n_{sink}} \tau P d_i^{DN}}{\sum_{i=1}^{n_{sink}} P d_i^{pcc}} \quad 5.12$$

Here, τ is the number of feeders used to form ADN. To analyze the impact of the increase in $\%ADN_{load}$ the total load at the PCC has been decomposed into two parts as (i). Fixed PQ load and (ii) ADN_{load}. The equivalent schematic representation of $T\&D$ model has been shown in Fig. 4. ATC is usually computed for transactions from one area (source) to another (sink). In this work, the impact on ATC has been assessed; therefore, the presence of ADN in the sink area has been considered. The ADN_{load} and its percentage in the sink area has been determined using the (5.10)– (2.58). The ADN comprises several $DERS$ such as $PV\ DER$, $WIND\ DER$, and $PV\&WIND\ DER$. The analysis presented in this chapter considers the deployment of CVR in the DN as a tool for optimal operation of ADN and subsequently assesses its impact on ATC at TN level.

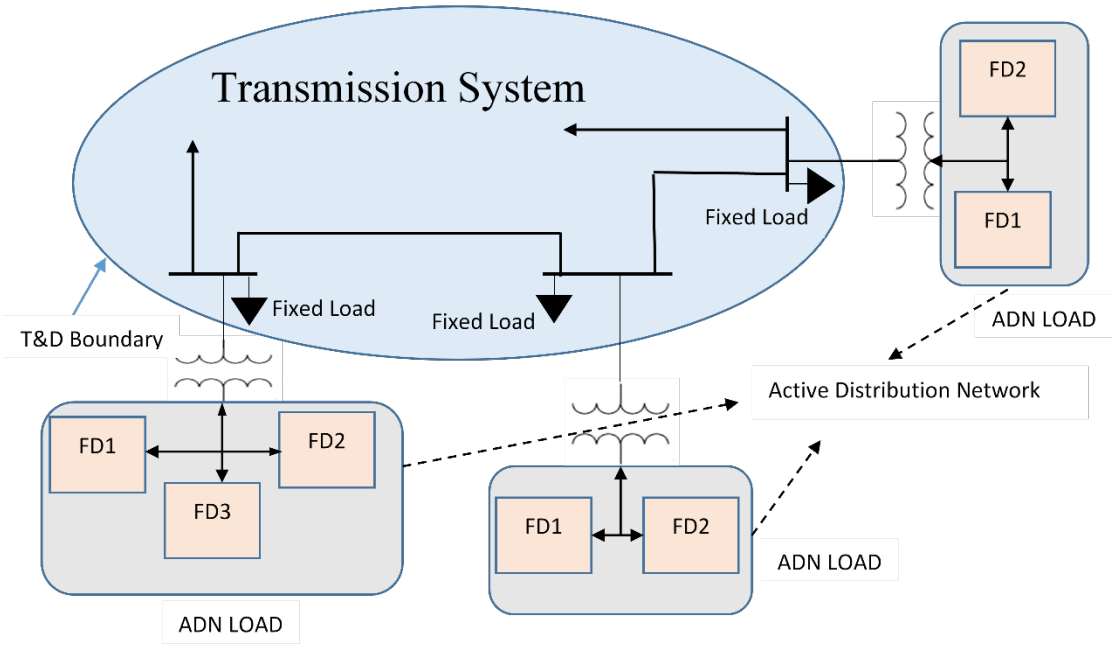

Figure 5.2 Diagrammatic representation of aggregated Model of T&D System.

5.4 ATC & CVR: A BRIEF OVERVIEW

5.4.1 ATC

The amount of power that can be transmitted over and above the existing transmission commitments while providing for the capacity benefit margin (CBM) and transient reliability margin (TRM) is defined as ATC [160]. ATC can be mathematically given as:

$$ATC = TTC - (CBM + TRM) - ETC \quad 5.13$$

In (2.58), TTC is the total transfer capability, and ETC is the existing transmission commitments. Contingencies play a major role in determining the appropriate ATC value; therefore, credible contingencies should be considered for assessing the ATC of the system.

At the transmission level, the transmission system operators (TSOs) strive to materialize a secure, economical, and reliable operation of TN with a flat voltage profile and stringent frequency regulation. On the other hand, the objective of the Distributed System Operator (DSO) is to operate the distribution network (DN) in such a way that the cost of operation and losses are minimum with redundant and reliable supply to the consumers. The DSO employs volt VAR optimization, CVR, network reconfiguration, demand response management, and other available techniques at their disposal to achieve their objectives. Some of the objectives may be contradictory at the transmission and distribution levels; for instance, CVR strives to operate the DN at the lower permissible limit of voltage deviation to facilitate demand reduction [121]; on the contrary, the TSO strives for a flat voltage profile through TNO (Transmission Network Optimizer). For proper functioning, the coordinated operation of the TSO and DSO should be performed so that the contradicting objectives could be dealt with appropriately. Also, the control

techniques adopted in ADN for VVO (Volt VAR Optimization) might as well affect the ATC of the TN; therefore, the VVO control implemented through CVR has been considered while formulating the problem for assessment of ADN impact on ATC.

5.4.2 CVR

The distribution feeders mostly have voltage-dependent type loads that are very sensitive to voltage variations. Many practical studies reveal that feeder load demand can be indirectly controlled by varying the voltage profile [122]. In this respect, the concept of (CVR) has been exploited to reduce the feeder peak load demand. Various studies on CVR have been conducted to analyze its effect [118]. However, most of the reported work deals with the CVR effect on energy savings in the distribution system. It is worth mentioning that very few have demonstrated the impact of CVR in the transmission system. The authors of [120] have studied the CVR effect on voltage stability of the transmission system, and the study reveals that voltage stability margin can be increased with the integrated operation of CVR. Motivated by the impact of CVR in voltage stability, in this study, the effect of CVR on ATC has been addressed. Various schemes are already available in the literature to enable the CVR operation. In this study, a smart grid-enabled CVR methodology has been utilized. Basically, this scheme executes the CVR operation through optimal settings of Volt/Var regulation devices. However, the optimal setpoints have been determined using a VVO engine operating with CVR as an objective function. In this work, the impact of enabling CVR is measured based on CVR savings, that is, the total reduction in power demand as defined under:

$$CVR^{savings}(\%) = \frac{(Power^{Base} - Power^{CVR})}{Power^{Base} \times 100} \qquad 5.14$$

where CVR^{saving} is percentage savings achieved, $Power^{Base}$ is total power consumptions in the base case or without CVR, and $Power^{CVR}$ represents the total power consumption after the CVR has been deployed. The CVR savings achieved based on (23) in distribution feeders will be aggregated, and its impact on ATC is further analyzed using the ITD platform.

5.4.3 Load model impact

Savings achieved through CVR is greatly influenced by the type of load, especially voltage-dependent loads. For load modeling, a method has been proposed in [161], [162] considering the practical aspects of user-end behavior. This study also utilizes a similar load model to build a relationship among load power demand, voltage, and CVR factor with exponential equations as delineated under

$$Pd_i^{DN}(t) = Pn_i^{DN}\left(\frac{V_{i,t}^{DN}}{Vn_{,i}^{Dn}}\right)^{CVR_{f(kW)}} \quad 5.15$$

$$Qd_i^{DN}(t) = Qn_i^{DN}\left(\frac{V_{i,t}^{DN}}{Vn_{,i}^{Dn}}\right)^{CVR_{f(kW)}} \quad 5.16$$

where $CVR_{f(kW)}$, and $CVR_{f(kVAR)}$; represents CVR factors in kW, and $kVAR$ and have been taken from [161].

5.5 PROBLEM FORMULATION: ADN IMPACT ON ATC

The overall problem of assessing the impact of deploying CVR in ADN on ATC involves the coordinated approach whereby the CVR at the distribution level and ATC at transmission-level are simultaneously evaluated. Therefore, the problem involves a platform that could facilitate the integrated operation and control of transmission and

distribution systems. The ITD platform proposed in section 5.2 has been used for this purpose. For simplicity of understanding, the problem is segregated into three sections: -

5.5.1 ATC: transmission level

5.5.1.1 *Stage 1: Real-Time Contingency Analysis:*

Real-time contingency analysis (RTCA) is a vital function of the modern energy management system. The RTCA is performed to identify the critical contingencies that would adversely affect the performance and reliability of the power system [137]. As optimization is not required for performing RTCA, the computing process does not enforce any constraints. In this chapter, the RTCA algorithm discussed in Chapter 2 section 2.5.4.3 has utilized for contingency ranking.

$$PI_c = \left[\sum_{i=1}^{N}\left(\frac{d_{v,i}^{l}}{g_{v,i}^{u}}\right)^{2n} + \sum_{i=1}^{N}\left(\frac{d_{v,i}^{l}}{g_{v,i}^{l}}\right)^{2n} + \sum_{i=1}^{N}\left(\frac{d_{p,i}}{g_{p,i}}\right)^{2n}\right] \quad 5.17$$

$$C = S_1^k\{PI_c\} \quad 5.18$$

In the above equations PI_c is the contingency index, d_{vi}^{u}, d_{vi}^{l} , g_{vi}^{l}, g_{vi}^{u} are the normalized upper and lower limit violations for the alarm and security limits, $d_{p,j}$, and g_{pj} stands for the normalized power flow limits, n is the normalization factor. The n is exponent used in hyper ellipse equation [163] and is taken as 2. The composite security index (5.17) is used for obtaining the contingency ranking. The contingency that has the highest index is most severe, and with one with the smallest value of the index is the least severe. Hence a set of credible contingencies (C) is formed using the function S_k^l which forms a set of 'k' credible contingencies that would be used for ATC assessment.

5.5.1.2 *Stage.2: ATC assessment and enhancement problem formulation:*

The ATC as given in (5.13) can be formulated as an optimization problem [160] and is given as $Max \sum_{i=1}^{N}(Pdi - Pd0i)$. The maximisation is achieved while maintaining the power system operational constraints within limits. The ATC in the system is affected by the presence of FACTS devices in the system. The ATC assessment formulation considering the impact of FACTS devices and considering the set of credible contingencies is given in (5.19).

$$Min\big(Max\, f(Pd, c, B_{SVC}, X_{TCSC})\big) \tag{5.19}$$

$$f(\cdot) = \{f_{c1}, f_{c2}, \dots f_{ck}\} \rightarrow k \; is \; number \; of \; critical \; contingency \tag{5.20}$$

$$f_{ck}(Pd, B_{SVC}, X_{TCSC}) = \sum_{I=1}^{N}\big(Pd_{i,t}^{TN} - Pd0_{i,t}^{TN}\big)\Big|_{under\; k^{th}\; contingency} \tag{5.21}$$

For $k = 1 \; to \; nc$ (number of credible contingencies considered from RTCA output). The optimization is achieved while maintaining the equality and inequality constraints $\mathcal{H}(x)$ and inequality constraints $\mathcal{G}(x)$ given in (5.22) to (2.58). The equality and inequality constraints inadvertently represent the impediments of the power flow (i.e.) power balance at each node along with the maximum and minimum limits on Voltages, Voltage angles, line flows, and generators) along with the upper and lower limits of compensation that could be provided by the FACTS devices

$$\mathcal{H}(x) = 0 \tag{5.22}$$

$$\mathcal{G}(x)^{min} \leq \mathcal{G}(x) \leq \mathcal{G}(x)^{max} \tag{5.23}$$

$$c_k \subset C \tag{5.24}$$

The $Min\ (Max)$ optimization given in (5.19) strives to maximize the ATC corresponding to each credible contingency available in the set of credible contingencies, provided by the RTCA and at the same time yields the minimum value of ATC. This is done because the ATC corresponding to the contingency, which would yield the minimum value of ATC, would be considered as the final value. If the system is scheduled considering minimum ATC and any other credible contingency happens, then the system would be able to operate reliably and securely. Contrarily, if the higher value of ATC is scheduled and the contingency corresponding to the minimum value of ATC happens, then the system will not be able to satisfy its operational commitments.

5.5.2 CVR: distribution level

The CVR is achieved at the distribution level through the ADMS by the DSO. The objective of the ADMS server is to minimize the load demand while enabling the CVR operation as given in (5.25) followed by system constraints as given hereunder.

5.5.2.1 *Objective function:*

$$\alpha_{Pd,t}^{DN} = min\left\{\sum_{i=1}^{n_w} P_{w,t}^{i} + \sum_{i=1}^{n_{pv}} P_{pv,t}^{i} - \sum_{i=1}^{l_d} P_{L,t}^{i} - P_{loss,total}^{ADN}\right\} \tag{5.25}$$

Here,

$$P_{loss,total}^{ADN} = \sum_{t=1}^{T}\sum_{q=1}^{F} P_{loss,q,t}^{DN} \tag{5.26}$$

$$\sum_{q=1}^{F} P_{loss,total}^{ADN} = \sum_{q=1}^{F}\left\{\begin{array}{c} G_{q,t}^{DN}\left[\left(\zeta_{ij,t}V_{i,t}^{DN}\right)^2 + \left(\zeta_{ji,t}V_{j,t}^{DN}\right)^2 - 2\zeta_{ij,t}V_{i,t}^{DN}\zeta_{ji,t}V_{j,t}^{DN}\cos(\theta_{ij,t})\right] \\ +G_{ij,T}^{DN,0}\zeta_{ij,t}\left(V_{i,t}^{DN}\right)^2 + G_{ij,t}^{DN,0}\zeta_{ij,t}\left(V_{i,t}^{DN}\right)^2 \end{array}\right\} \tag{5.27}$$

Where $q = i - j$ (i.e., the link connecting node $i\ to\ j$). Further, in the following equation $Y_{ij,t}^{DN} = G_{ij,t}^{DN} + jB_{ij,t}^{DN}$.

$$g_{ij,t} + jb_{ij,t} = \begin{cases} \sum_{j \in J} \zeta_{ij,t}^2 \left(Y_{ij,t}^{DN} + Y_{ij,t}^{DN,0}\right), i = j \\ -\zeta_{ij,t}\zeta_{ji,t} Y_{ij,t}^{DN} \quad , i \neq j \end{cases} \quad 5.28$$

5.5.2.2 *Constraints:*

The objective mentioned in (5.25) have been met while adhering to the impediments delineated in the following equations

$$V_{i,t}^{min,DN} \leq V_{i,t}^{DN} \leq V_{i,t}^{max,DN}$$
$$i.e. \widetilde{0.95} \leq V_{i,t}^{DN} \leq \widetilde{1.05} \quad 5.29$$

$$P_{i,t}^{min,DN} \leq P_{i,t}^{DN} \leq P_{i,t}^{max,DN} \quad 5.30$$

$$Q_{i,t}^{min,DN} \leq Q_{i,t}^{DN} \leq Q_{i,t}^{max,DN} \quad 5.31$$

$$P_{i,t}^{DN} = P_{Gi,t}^{DN} - P_{Li,t}^{DN} = \sum_{j}^{J} V_{i,t}^{DN} V_{j,t}^{DN} (g_{ij,t}\cos(\theta_{ij,t} + b_{ij,t}\sin(\theta_{ij,t}) \quad 5.32$$

$$Q_{i,t}^{DN} = Q_{Gi,t}^{DN} - P_{Li,t}^{DN} = \sum_{j}^{J} V_{i,t}^{DN} V_{j,t}^{DN} (g_{ij,t}\cos(\theta_{ij,t} - b_{ij,t}\cos(\theta_{ij,t}) \quad 5.33$$

$$Q_{i,t}^{cb} = \beta_{i,t}^{cb} \Delta q_{i,t}^{cb}; \beta_{i,t}^{cb} = \{0,1,2, \dots \beta_{i,t}^{cb,max}\} \quad 5.34$$

$$\left.\begin{array}{l} \gamma_{tr,t} = 1 + tap_{tr,t} \dfrac{\Delta V_{tr,t}}{100} \\ where, \Delta V_{tr,t} = 0.03125 \end{array}\right\} OLTC/Regulator \quad 5.35$$

In addition to the above impediments, the constraints discussed in ADS Modelling have also been met.

5.5.3 Combined transmission & distribution: ITD objective

The objective function for this stage is an amalgam of the two parts discussed in the previous sections and can be defined in (2.58)

$$\begin{aligned} &Min(Max\ f(Pd, \alpha_{Pd_i}^{DN}, c, B_{SVC}, X_{TCSC}, cb, tap) \\ &f(\cdot) = \{f_{c1}, f_{c2}, \dots f_{ck}\} \rightarrow k\ is\ number\ of\ critical\ contingency \end{aligned} \tag{5.36}$$

$$f_{c_i}(\cdot) = \left(\begin{array}{c} \left\{ \sum_{i=1}^{N_{sink}} \left(Pd_{i,t}^{TN} - Pd0_{i,t}^{TN} \right)|_{i \in TN} \right\} I \\ + \\ \left\{ \sum_{i=1}^{N_{ADN}} \left(\alpha_{Pd_{i,t}}^{DN} - \alpha_{Pd0_{i,t}}^{DN} \right)|_{i \in ADN} \right\} II \end{array} \right) \Bigg|_{i \in [1, n_c]} \tag{5.37}$$

The objective of overall ITD operation (5.36) has been met by adhering to the impediments of both ATC evaluation and CVR deployment problems (5.25) to (5.27) and (5.29) to (5.35).

5.5.4 Optimization technique

The objective function of ITD (i.e., ATC assessment in the presence of ADN) has been solved by employing pattern search optimization. The details of the pattern search optimization technique could be found in chapter 1. Particle swarm optimization has been used as an alternative optimization technique to corroborate the pattern search technique's results.

5.6 IMPLEMENTATION OF THE PROPOSED METHOD

The ITD Framework developed in this chapter has been used for analyzing the ITD system. The functioning of MAS employed in the integrated analysis and the solution methodology have been discussed hereunder.

5.6.1 Functioning of MAS

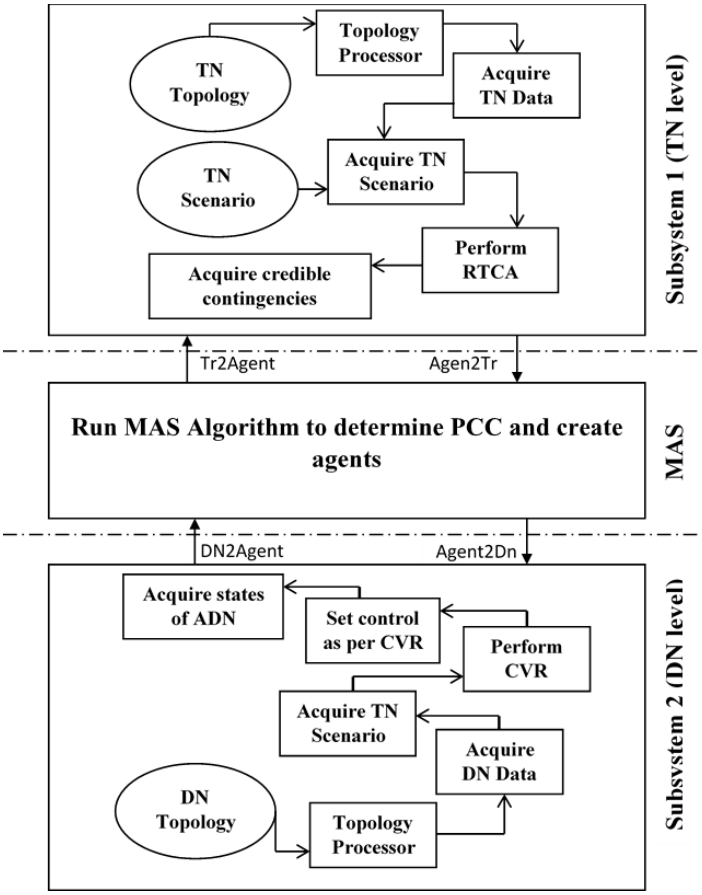

Figure 5.3 Schematic representation of MAS functioning in ITD implementation.

The ITD Framework illustrated in Figure 5.3 consists of two subsystems (subsystem 1 & subsystem 2) $subsystem\ 1$ represents the TN level, and $subsystem\ 2$ represents the DN level. These two systems interact through the MAS system while using $tr2agent/\ agent2tr$ and $dn2agent/agent2dn$ protocols. The overall process of MAS interaction with TN and DN has been delineated as under:

5.6.1.1 *Multi-agent System:*

The MAS acquires the data $to\ and\ fro$ from the TN and DN depending upon the mode of operation. It runs the MAS algorithm (Table 5.1) to determine the PCC/ADN nodes of the TN and creates the agents of MAS.

5.6.1.2 *Subsystem1:*

At the TN level (Subsystem 1), different components such as Topology Processor and RTCA have been deployed. In Figure 5.3, information flow between various blocks at the TN level has been shown. The detailed flow chart and process flow have been explained in Fig. 6. At the TN level, the admittance matrices are formed for the TN topology through the Topology processor, and primitive TN data is formed.

Table 5.1 Implementation algorithm of MAS system

Steps	**Description of steps**
Step 1	Specify the ADN nodes in the transmission network.
Step 2	Surf the TN Topology and designate the ADN nodes as PCC.
Step 3	Allocate agents for designated PCC's in MAS (Multiagent System).
Step 4	Select the operating mode of MAS.
Step 5	Access the measured states $(P, Q, V, \delta, DN_{loses}, taps, caps)$ from DSO using $dn2agent$ protocol into MAS agent vectors.
Step 6	Communicate the data from the MAS agent vectors to the PCC of TN through $agent2tr$ protocol.

The TN scenario is used with this primitive data, and the set of credible contingencies are evaluated using the RTCA. The MAS acquires the information of sink and source area (comprising of load, generation, and PCC for ADN).

5.6.1.3 *Subsystem2:*

The $Subsystem2$ represents the DN level that employs DSO for solving the DN. At the DN level, the primitive DN data is formed using the DN topology. The DN scenario is added to this primitive data to form the complete DN data. The ADN states are obtained

by solving the DN with and without the consideration of CVR (as the case may be) using the complete DN data. If CVR is considered, then the capacitor and transformer taps are set according to CVR; otherwise, their predefined default values have been used.

The $Subsystem1$ is a built-in $MATLAB$ environment where the TN has been modeled, while $Subsystem2$ has been built using $OPENDSS$ software in which the ADNs have been modeled. The MAS system developed using $MATLAB$ has been used to materialize the integrated operation of both the transmission and distribution system. During the optimization process, part II of the O.F has been obtained at subsystem 2 (DN level), and the part I has been provided by subsystem 1 (TN level) through proper interaction and data exchange between the two subsystems.

5.6.2 Solution methodology

The algorithm used for the implementation of the proposed method has been inked in Figure 5.4. The figure primarily shows coordinated processes happening at two different levels, which are interacting with each other using the MAS interface discussed in Section 7.1.

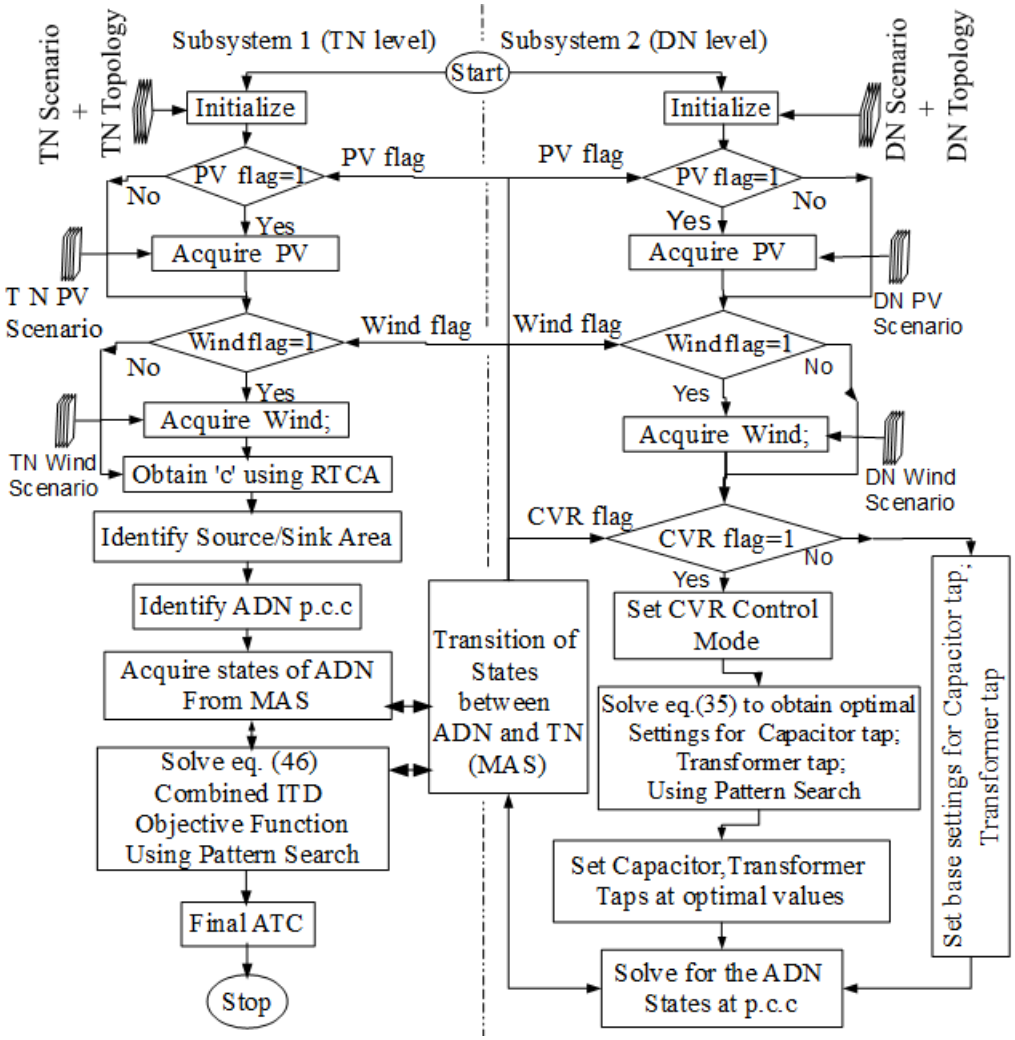

Figure 5.4 Algorithm flowchart for an implementation of the proposed method.

MAS has been used for the transition of states between $subsystem\ 1$ and $subsystem\ 2$. Block 'Initialise' shown in Figure 5.4 forms the complete TN and DN data (using the Topology Processor, Acquire TN/DN data, Acquire TN/DN scenario Figure 5.3). Depending upon the flags (PV, Wind), the PV and Wind are incorporated in the solution process using the models discussed in section 5.3.1.1 and 5.3.1.2. If the flag is unity, the PV and Wind are considered; else, they are discarded. At TN level RTCA is utilized to obtain a set of credible contingencies c followed by identification of source, sink and the pcc $(ADN\ node)$. This information is commuted to DN level through the

MAS. At DN level if CVR flag is unity the (5.25) is solved and the taps of capacitors and transformers are set as per CVR; otherwise, default values of taps are used. At this stage, DN is solved, and the $ADN\ states$ (ADN_{load}) are commuted to TN level through MAS (α_{Pd}^{DN}). At TN level these states are acquired and (5.36) is being solved using pattern search optimization to yield the final ATC value.

5.7 CASE STUDY: RESULTS AND DISCUSSION

The developed method has been utilized for integrated analysis of the ITD system whereby Modified IEEE 24-BUS RTS has been considered at transmission-level and Modified IEEE 123 bus feeder has been considered at the distribution level.

5.7.1 Description of the test system

5.7.1.1 *IEEE modified 24 BUS RTS:*

The IEEE 24 bus system has been modified and bifurcated into three different areas A1, A2, and A3, respectively. The ATC has been evaluated for transactions from one area (source area) to another area (sink area). The load nodes of the sink area have been taken as sink nodes; some of these nodes have been set as pcc. The total load of this pcc has been decomposed into two parts, i.e., (i) Fixed PQ and (ii) ADN load. The ADN load (variable) comprises IEEE 123 bus distribution systems. The source generator buses of the source area have been taken as source nodes. The incremental load in the sink area has been compensated by the equivalent increase in the generation of the source area.

Table 5.2 Description of the test system

Hierarchy	Case	Area	Generator Bus	Load Bus	Gen Cap (MW)	Load (MW)	Margin (MW)	AGC (MW)
	IEEE 24 BUS RTS	1	[14;15;16;18;21]	[14;15;16;18;19]	1170	1125	45	865
		2	[13,22,23]	[5;6;8;9;10;13;20]	1551	1141	410	515
		3	[1;2;7]	[1,2,3,4,7]	684	584	100	176
DN Level (5 % ADN Load)	IEEE 123 BUS Distribution	ADN/PCC	Fixed Load		Active Load		DER (Gen Cap)	
			P	Q	p	Q	WIND (MW)	PV (MW)
							(Max)	(Max)
		5	67.7145	12.8839	16.4274	5.58048	10	6.5
		6	132.715	26.8839	16.4274	5.58048	10	6.5
		8	167.715	33.8839	16.4274	5.58048	10	6.5
		9	171.715	34.8839	16.4274	5.58048	10	6.5
		10	191.715	38.8839	16.4274	5.58048	10	6.5
		13	261.715	52.8839	16.4274	5.58048	10	6.5
		20	124.715	24.8839	16.4274	5.58048	10	6.5

The description of the complete test system (both TN and DN levels) has been depicted in Table 5.2. The modification done to the IEEE 24 Bus system is given in Table 2.1 whereas the tie lines interconnecting the three areas are portrayed in Table 2.2. Additional modifications are done by considering an SVC to be placed at bus 24 and TCSC being placed in L19, which connects Bus11 and Bus14. The compensation provided by SVC is of range −40/60 $MVAR$ while TCSC can provide up to a max of 20% of the line to which it is connected. PV system of 10 MW is connected at Bus9 in area 2 (A2), comprising of 275 modules of PV arrays (each module consisting of 52 PV panels), 5 connected in series and 55 in parallel. The parameters of the PV panel used in this work are given in Table 5.3 [160].

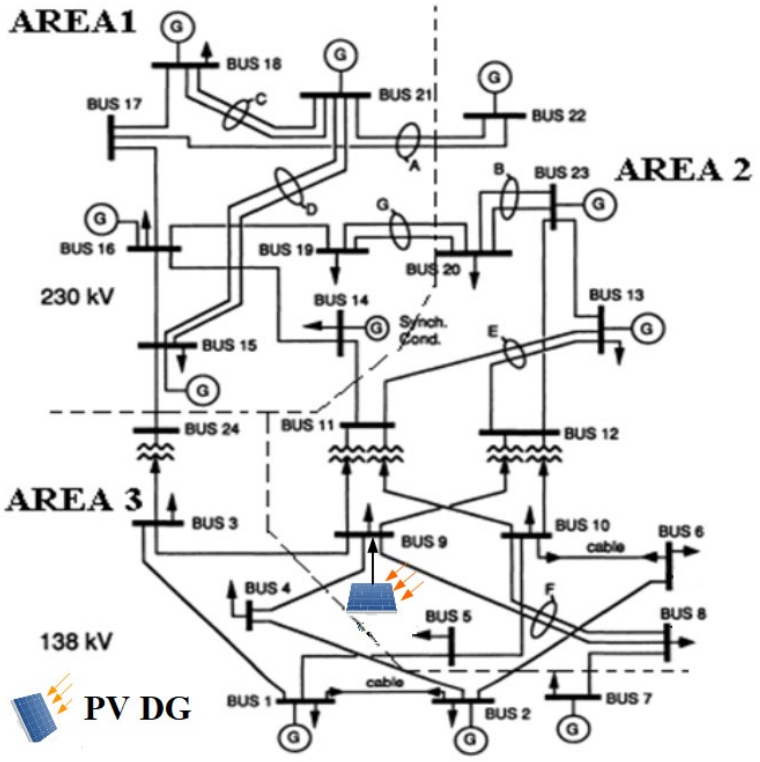

Figure 5.5 RTS 24 BUS Test System

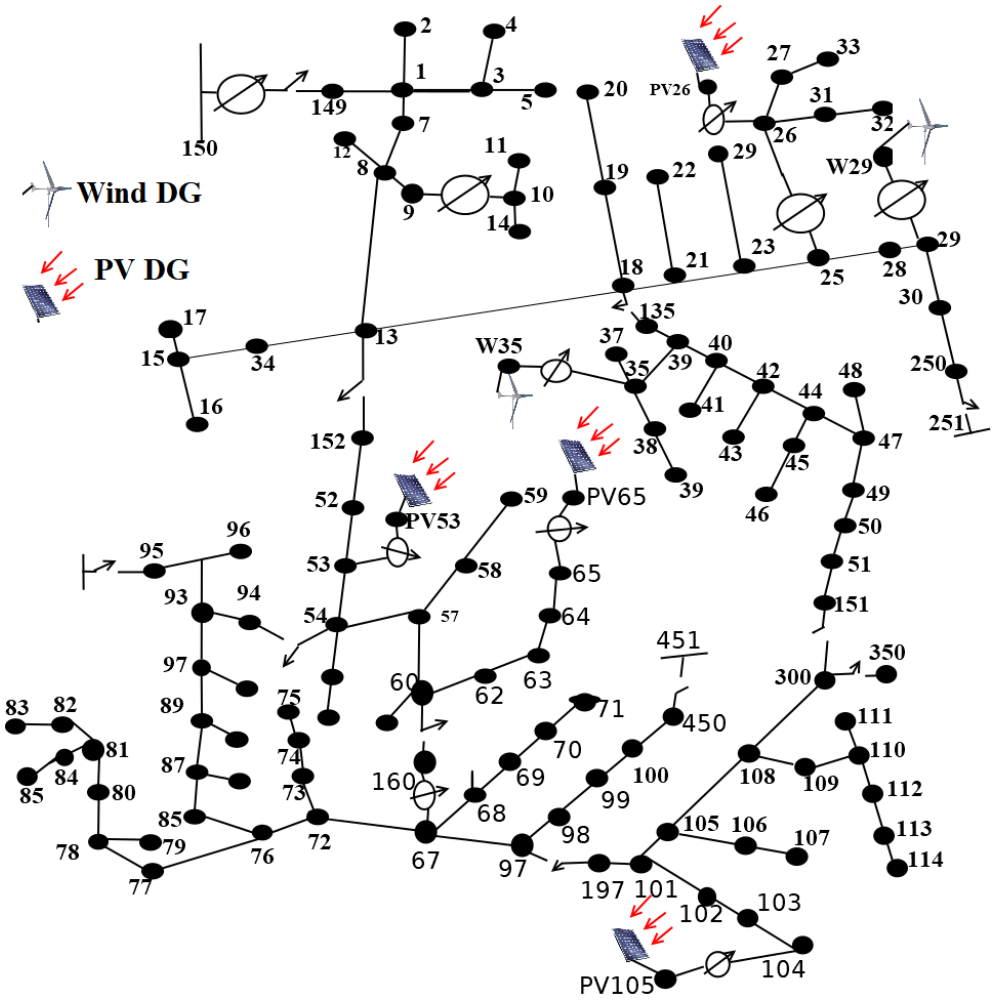

Figure 5.6 Modified IEEE 123 bus distribution test Feeder.

5.7.1.2 *IEEE 123 bus feeder:*

As the objective of this investigation is to assess the impact of ADN on ATC, a portion of the total load at the PCC has been represented by ADN. The ADN is formed by clusters of Modified IEEE 123 bus feeders. The number of feeders in the cluster is determined by the percentage of $\%ADN_{load}$ considered. The ADN_{load} and its percentage in the sink area is determined using (5.12). The additional modifications are done in IEEE 123 bus test system in terms of integrating the $DERS$ which are given hereunder (Figure 5.5 and Figure 5.6): -

1) Solar PV with smart inverters at bus 104 with a maximum capacity of 100 kW and at buses 26, 65, and 53 with a maximum capacity of 400 kW each as given in Table 5.3.
2) Wind Farm at buses 29 and 35 with a maximum capacity of 1000 kW each as given in Table 5.3.

Table 5.3 Description of DERs considered in ADN (Modified IEEE 123)

Se No	Bus	Type	Phases	Rating	PF
1	29	WIND	3	1000 kW	1
2	35	WIND	3	1000 kW	1
3	104	PV	1	100 kVA	0 to 0.9676
4	26	PV	3	400 kVA	0 to 0.9676
5	65	PV	3	400 kVA	0 to 0.9676
6	53	PV	3	400 kVA	0 to 0.9676

5.7.2 Results and inferences

The test system described in the previous section has been used whereby the proposed ITD platform has been employed for assessing the impact of ADN on ATC. The impact of ADN has been performed at different levels of ADN percentage along with the impact of deploying CVR in the ADN. Various aspects of ADN assessed using the ITD platform are:

- Impact of increasing the $\%ADN_{load}$ in the sink area.
- Impact of the presence of PV DER.
- Impact of the presence of WIND DER.
- Impact of the presence of both WIND&PV DER.

- Impact of deploying CVR in the ADN.

At first, the performance of pattern search optimization for ATC assessment have been discussed and subsequently the effect of FACTS devices on ATC, the impact of deploying CVR in ADN, the effect of varying the $\%ADN_{load}$ is presented.

5.7.2.1 *Optimization results*

The ATC for transactions from A1 to A2 has been evaluated using the pattern search optimization discussed in Section 5.5.4. The termination criterion of the process has been defined in terms of mesh size (taken as $\mathbf{1 \times 10^{-10}}$). The convergence of the proposed technique has been shown in Figure 5.7, where the current mesh size, best function value, and total function count have been shown. The pattern search optimization being a direct search technique, is capable of reaching the global optimal in each run and produces the same solution for multiple runs. Further, the nature of the problem is such that the direction in which the solution would be obtained is known with a probable linear link with the variable (i.e., would increase if the variable is increased); therefore, in such case, the proposed method performs better. Results obtained by pattern search (PS) optimization are corroborated for its performance by comparison with particle swarm optimization technique (PSO). Figure 5.8 shows the convergence of PSO, while the comparative result for both the methods (PS & PSO) have been shown in Figure 5.7, where ATC value and computational time have been taken as the basis of comparison. The ATC value has been computed for the same case in multiple runs using both techniques Table 5.4.

.

Table 5.4 Comparison of pattern search and PSO technique.

Se. No	Pattern Search		Particle Swarm	
	ATC, MW	Time, s	ATC, MW	Time, s
1	235.64	1.53	235.06	23.69
2	235.64	1.58	235.22	25.53
3	235.64	1.6	235.55	72.93
4	235.64	1.99	235.12	28.92
5	235.64	1.86	235.49	51.38

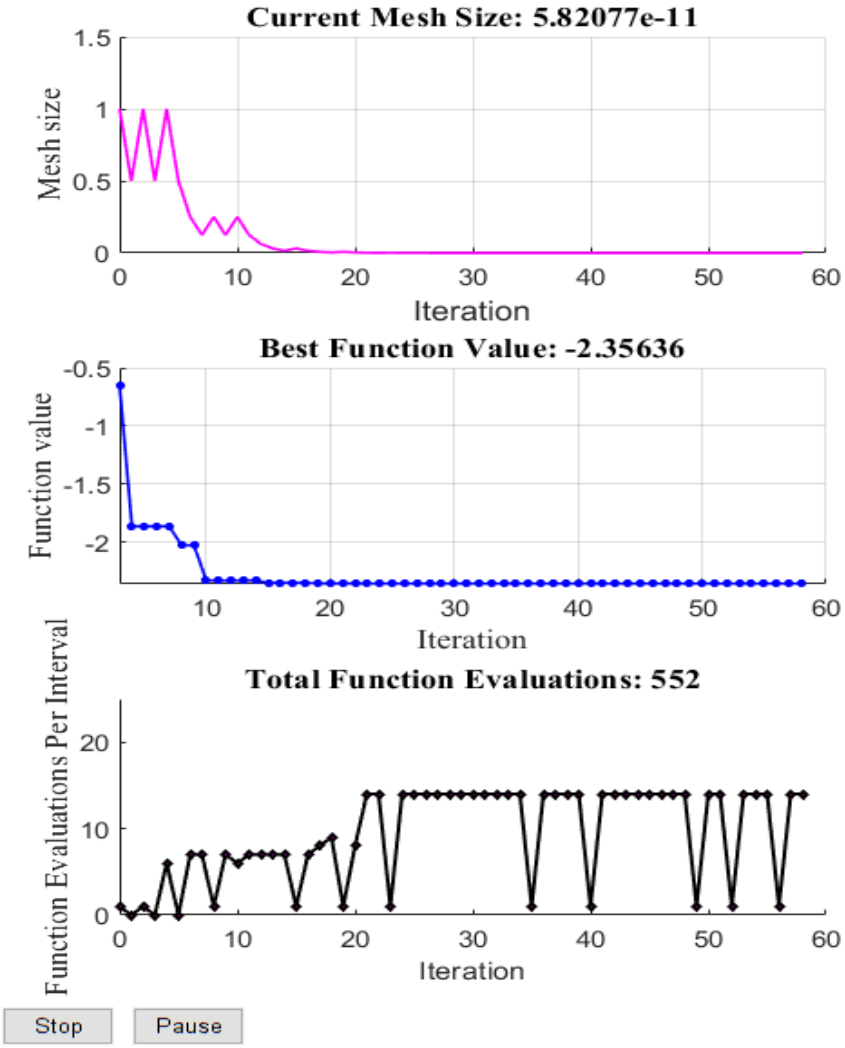

Figure 5.7 Convergence of pattern search optimization.

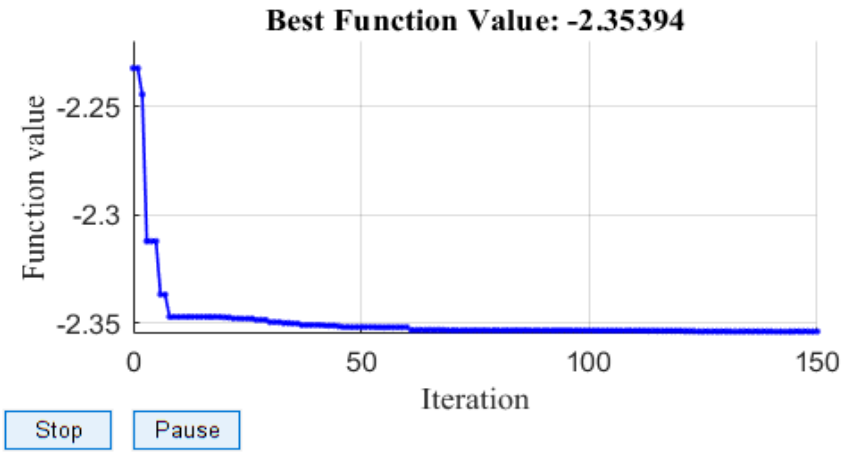

Figure 5.8 Convergence of particle swarm optimization.

From the table, it could be observed that the PS produces a higher ATC value as compared to the PSO. The PS is computationally efficient as it takes much less time than PSO and produces the same optimal result in multiple runs.

5.7.2.2 *Effect of FACTS devices:*

The presence of FACTS devices enhances the ATC of the system. The results of ATC estimation with and without the FACTS devices have been obtained and tabulated in Figure 5.8. The Table 5.5 shows ATC values for different cases whereby absence (0) and presence (1) of FACTS device, CVR, and DER have been considered. The ATC shown is for transactions from A1 to A2 in the Modified IEEE 24 bus RTS system. It can be observed that the FACTS devices improve the ATC value. When no FACTS device is considered, then the ATC is computed as 188.06, which is smaller than that computed in the presence of FACTS device, i.e., 195.38 with only SVC and 198.54 when both SVC and TCSC are present.

Table 5.5 Results illustrating the effect of considering the FACTS devices on the ATC of the system.

S.No	FACTS		CVR	DER		ATC, MW
	SVC	TCSC		PV	WIND	
1	0	0	0	0	0	188.06
2	1	0	0	0	0	195.38
3	1	1	0	0	0	198.54
4	1	1	1	0	0	202.14
5	1	1	1	1	0	215.98
6	1	1	1	1	1	235.64

5.7.2.3 *Impact of CVR at 5% of* $\%ADN_{load}$*:*

The truth table representation of different cases has been illustrated in Table 5.6. The table contains five columns; among them, the first contains the serial/case number, while the other three contain the flag for CVR, PV, and Wind. The cell containing the flag value unity indicates that the case (row) to which the cell belongs considers the effect of quantity present in the column to which the cell belongs. The ATC results under different cases for quasi-static simulation (24 h) of the integrated system is shown in Figure 5.9. The ATC considering the impact of CVR corresponding to peak hour has been depicted in Table 5.6. As shown in Figure 5.9, the different cases are represented by the combinations of the flag present in that case, as shown in the legend. For instance, flag combination (000) belongs to the first case hence the symbol indicated by (000) in the legend corresponds to Case1 in which neither CVR nor PV and Wind presence has been considered. The following major inferences can be made:

Table 5.6 ATC under various cases at 12:00 pm peak load time for 5 % ADN_{load}.

S No	CVR	PV	WIND	ATC, MW	Evaluation Time, s
Case 1	0	0	0	251.15	2.19
Case 2	1	0	0	252.72	35.71
Case 3	0	1	0	289.63	2.85
Case 4	1	1	0	296.06	46.99
Case 5	0	0	1	278.17	2.32
Case 6	1	0	1	283.88	144.15
Case 7	0	1	1	297.95	2.49
Case 8	1	1	1	302.52	149.22

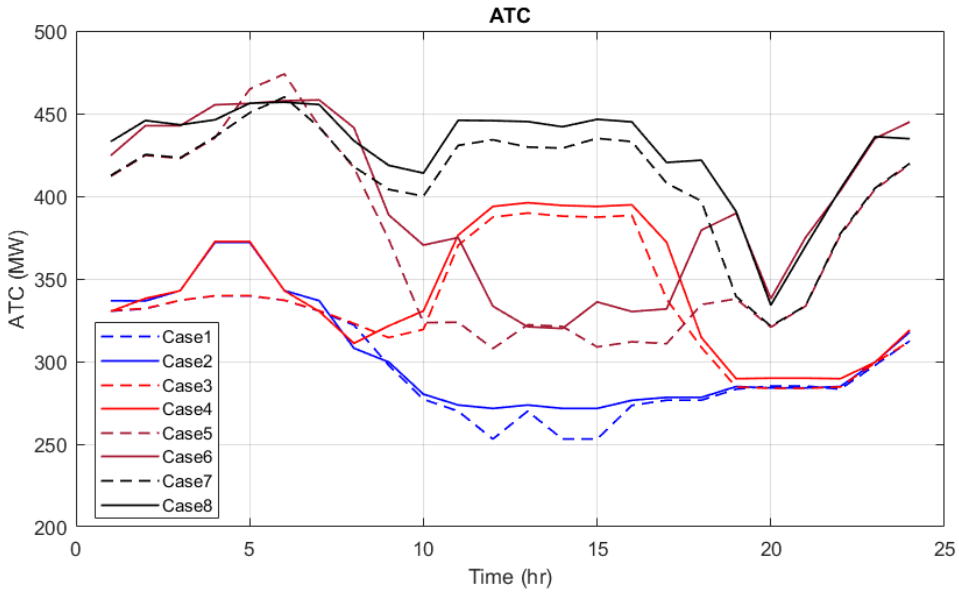

Figure 5.9 ATC variation for 24 h under various cases.

5.7.2.3.(i) Analysis Without CVR:

- As is evident from the response of the system for cases 1, 3, and 7, it can be inferred that the ATC of the system is affected by the presence and absence of the DER′s in the ADN.

- The ATC of the system considering PV (case 3) in ADN is higher than the base case.
- The ATC of the system considering Wind (case 5) in ADN is higher than the base case.
- The ATC of the system considering only PV (case 3) may be higher or less than the ATC of the system when only Wind (case 5) has been considered.
- Though the active power produced by the PV source is zero during night hours, there is an improvement in ATC. This could be attributed to the reactive power provided by the smart inverter present at the PV installation sites, along with the reduction in active and reactive power during the night hours.
- From the ATC of the system considering only Wind (case 5), it is evident that the ATC of the system is lesser than the case when only PV (case 3) is present typically during night hours, which could be attributed to the reactive power support capability of the smart inverters present at the PV installations.

5.7.2.3.(ii) Analysis With CVR:

- The ATC of the system has been improved in all the cases considered when CVR is implemented by the DSO.
- The ATC value is maximum when for (case 8) in which the flags for PV, Wind, and CVR are unity. (i.e., CVR implemented, while considering PV and Wind).
- ATC is higher when DER (PV & WIND) are present, and it has been further improved by deploying CVR. Deploying CVR would result in an increase in the mean value of ATC Figure 5.10 throughout the day.

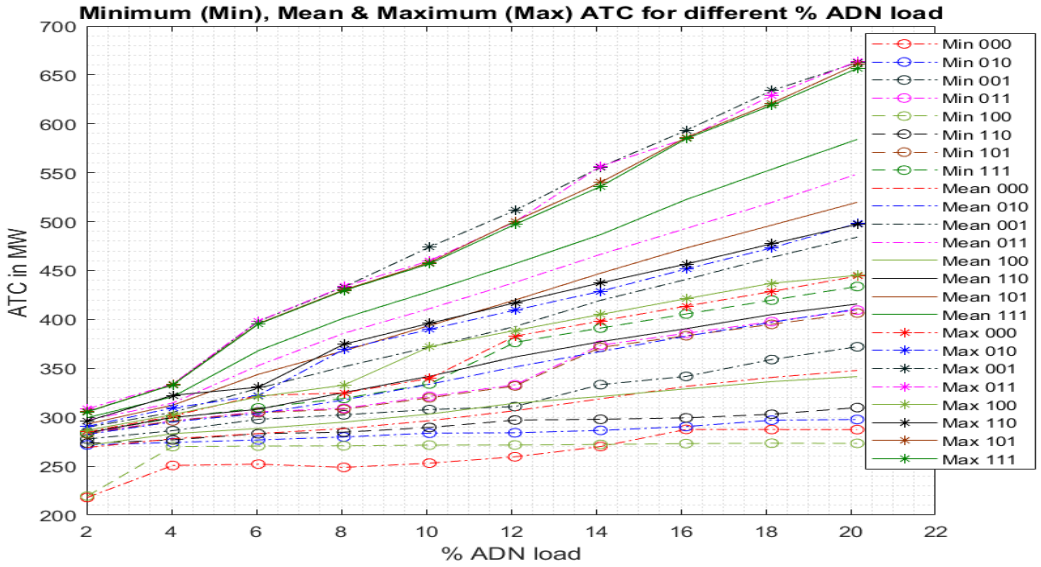

Figure 5.10 Minimum, maximum, and mean ATC value of different $\%ADN_{LOAD}$.

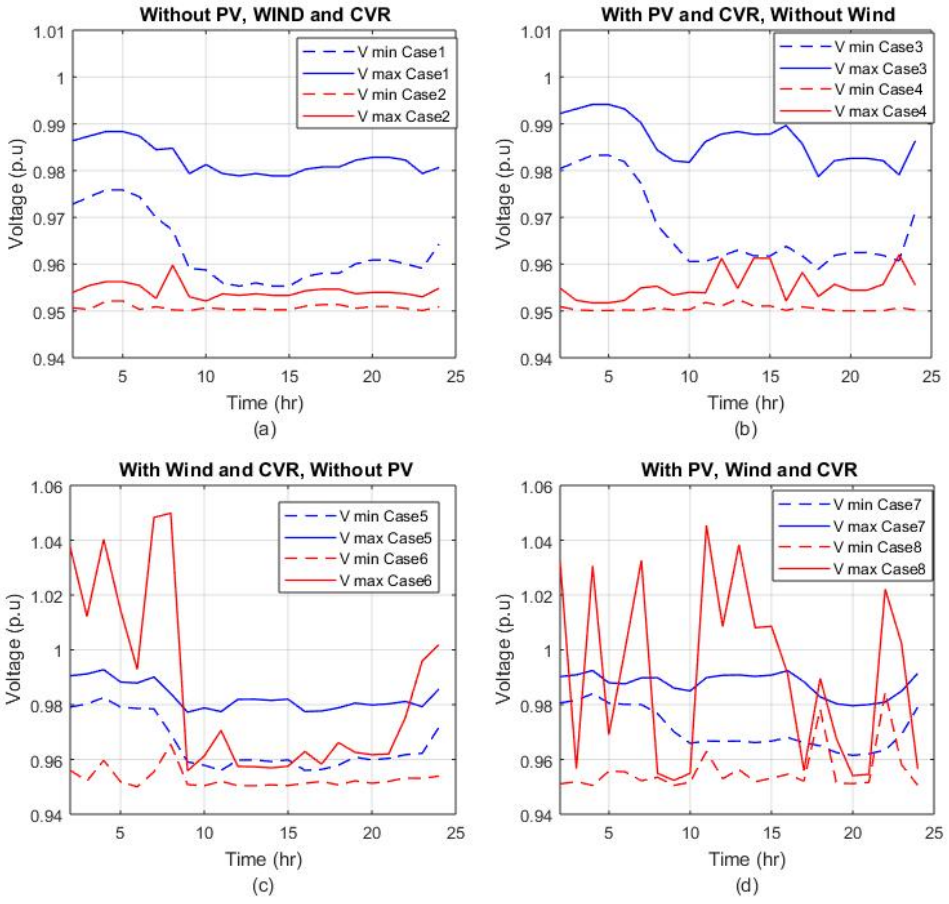

Figure 5.11 Minimum Voltage Profile of ADN for (a). Case1(000) and Case2(100) (b). Case3(010) and Case4(110) (c). Case5(001) and Case6(101) (d). Case7(011) and Case8(111).

The analysis of the test systems reveals that there has been an increment in ATC value with the inclusion of DERs and implementation of CVR. The minimum voltage of ADN has been given in Figure 5.11, and Figure 5.12 gives the CVR savings. It can be inferred that deployment of CVR brings down the minimum as well as maximum operating for voltage, as shown in Figure 5.11(a) and Figure 5.11.b for cases (1 to 4) Presence of Wind DER Figure 5.11(c) and Figure 5.11(d), results in higher maximum voltages but (at some instants) but the minimum voltage remains lower than the corresponding No-CVR case.

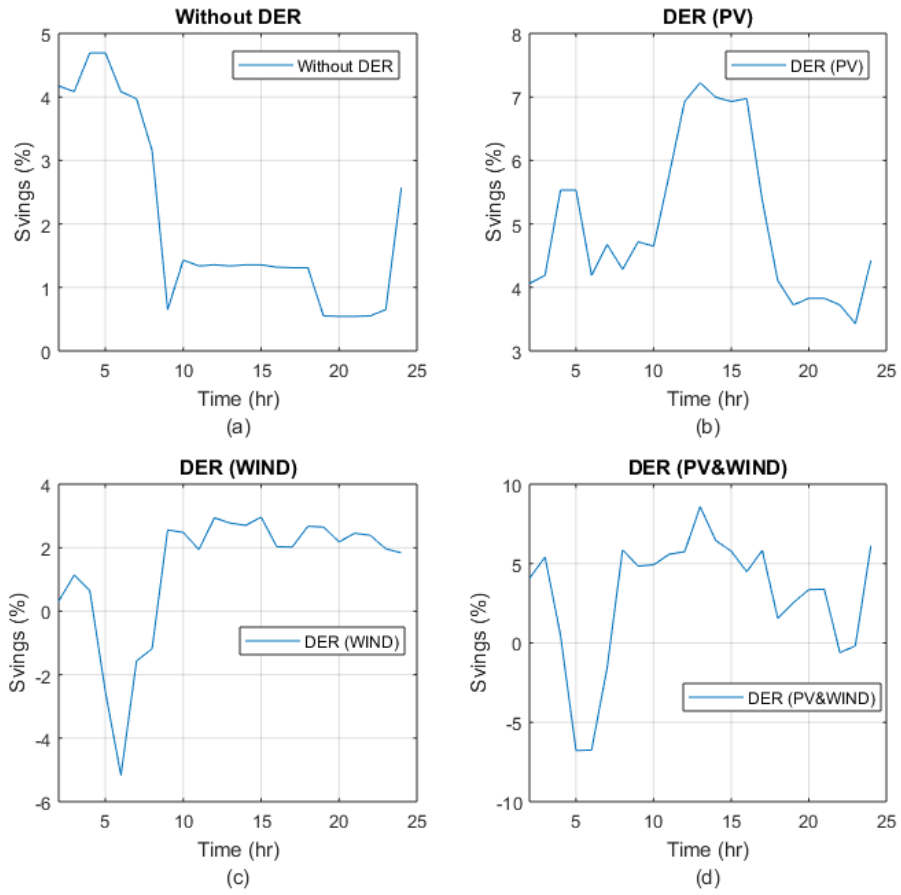

Figure 5.12 CVR Saving in percentage for different cases.

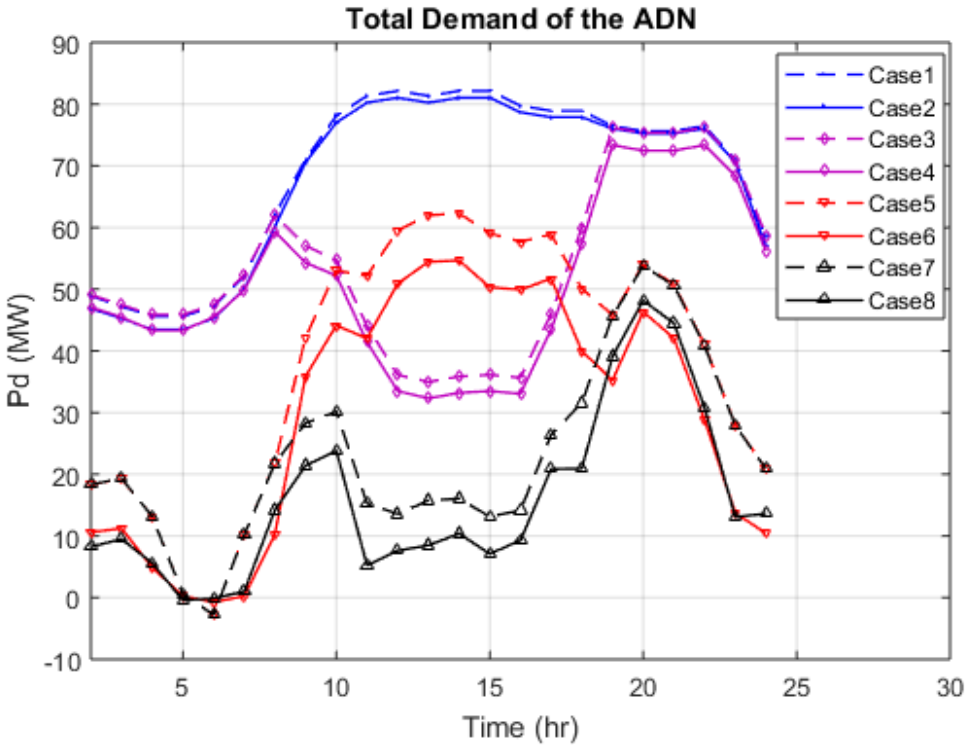

Figure 5.13 Quasi-static variation of a total load of ADN in the sink area.

The overall CVR saving due to the injection of DERs happens to be higher than the CVR savings without DER. During lower loading conditions (night hours) at some instants, the CVR saving becomes negative (Figure 5.12.c and Figure 5.12.d) under the presence of Wind-based DER. Further, from Figure 5.13, it can be inferred that at lower loading conditions, there happens to be the reversal of power flow from ADN to the TN through the PCC. The instants of the reversal power flows are those where the total ADN load becomes negative because of the higher penetration of power from DERs (Wind and PV).

Table 5.7 Minimum, maximum, and mean values of ATC.

S.No			1	2	3	4	5	6	7	8	9	10
	% ADN_{Load}		2.02	4.03	6.05	8.06	10.08	12.09	14.11	16.13	18.14	20.16
	(%) Fixed Load		97.98	95.97	93.95	91.94	89.92	87.91	85.89	83.88	81.86	79.84
Without CVR	Without DER	**Min ATC**	218	250.8	252.1	248.8	253.1	259.64	270.13	287.61	287.5	287.4
		Max ATC	285.1	301.2	322.3	324.9	339.71	382.92	398.44	413.67	428.6	444.4
		Mean ATC	269.1	278.1	283.4	288.5	296.51	306.73	318.84	331.64	340.74	347.9
	DER PV	**Min ATC**	271.8	274.3	276.8	279.9	283.77	284.18	286.63	290.51	297.03	297.8
		Max ATC	290.7	309.6	322.3	369.6	389.82	409.55	428.78	451.61	473.12	498.2
		Mean ATC	282.5	295.3	303.8	317.7	333.74	351.46	367.25	382.96	397.07	410.7
	DER WIND	**Min ATC**	277.7	286.4	297.9	302.5	307.86	310.97	333.39	341.82	359.04	372.1
		Max ATC	305.8	333.6	398.1	433.2	473.95	511.42	555.89	593.29	633.85	662.8
		Mean ATC	289.9	305.1	329.7	351.7	371.81	392.78	419.57	440.89	463.48	484.2
	DER-PV & WIND	**Min ATC**	284.1	296.4	305.7	309.1	321.4	333.25	373.74	385.87	397.81	409.6
		Max ATC	308.7	334.1	398.4	433.7	460.01	499.72	556.73	584.79	629.19	663.8
		Mean ATC	297.2	314.6	352.9	385.9	411.02	437.87	466.51	493.05	519.64	548.6
Without CVR	Without DER	**Min ATC**	219.4	270.1	270.6	270.9	271.6	271.69	272.26	273.12	273.52	273.3
		Max ATC	286.7	302.8	320.9	333	372.02	388.72	405.12	421.22	437.01	445.1
		Mean ATC	271.2	283.2	288.6	295.1	303.27	314.44	321.25	329.07	336.5	341.6
	DER PV	**Min ATC**	273.4	276.9	283.2	284.8	289.61	297.16	297.94	299.42	303.11	309.9
		Max ATC	296.1	322.5	330.7	374.6	396.07	416.99	437.41	456.65	477.34	497.2
		Mean ATC	284.2	299.9	308.1	325.3	341.93	361.67	377.28	390.55	405.04	415.8
	DER WIND	**Min ATC**	283.1	296.3	304.8	308.2	319.94	332	371.46	383.33	395.04	406.6
		Max ATC	305.7	333.4	395.7	430.2	458.22	500.5	540.08	586.02	621.07	660.8
		Mean ATC	293.1	312.4	343.9	367.9	393.77	419.83	447.26	473.02	496.35	519.8
	DER-PV & WIND	**Min ATC**	284.1	299.4	309.6	319.3	334.07	376.6	391.21	405.61	419.76	433.7
		Max ATC	305.5	333.2	395.2	429.6	456.9	497.18	535.95	584.71	618.94	656.6
		Mean ATC	299.6	321	368	401.4	428.55	457.06	486.67	522.56	553.51	584.1

5.7.2.3.(iii) Impact of increasing $\%ADN_{load}$:

ATC depends on the spatial dispersion of generation and load in the power network; therefore, the changes in the states of ADN due to variation in DN load profile, and presence of DER such as PV, WIND, WIND&PV reflects into the values of ATC. The minimum, maximum, and mean values of ATC that have been evaluated for 24 h duration is given in Table 5.7.

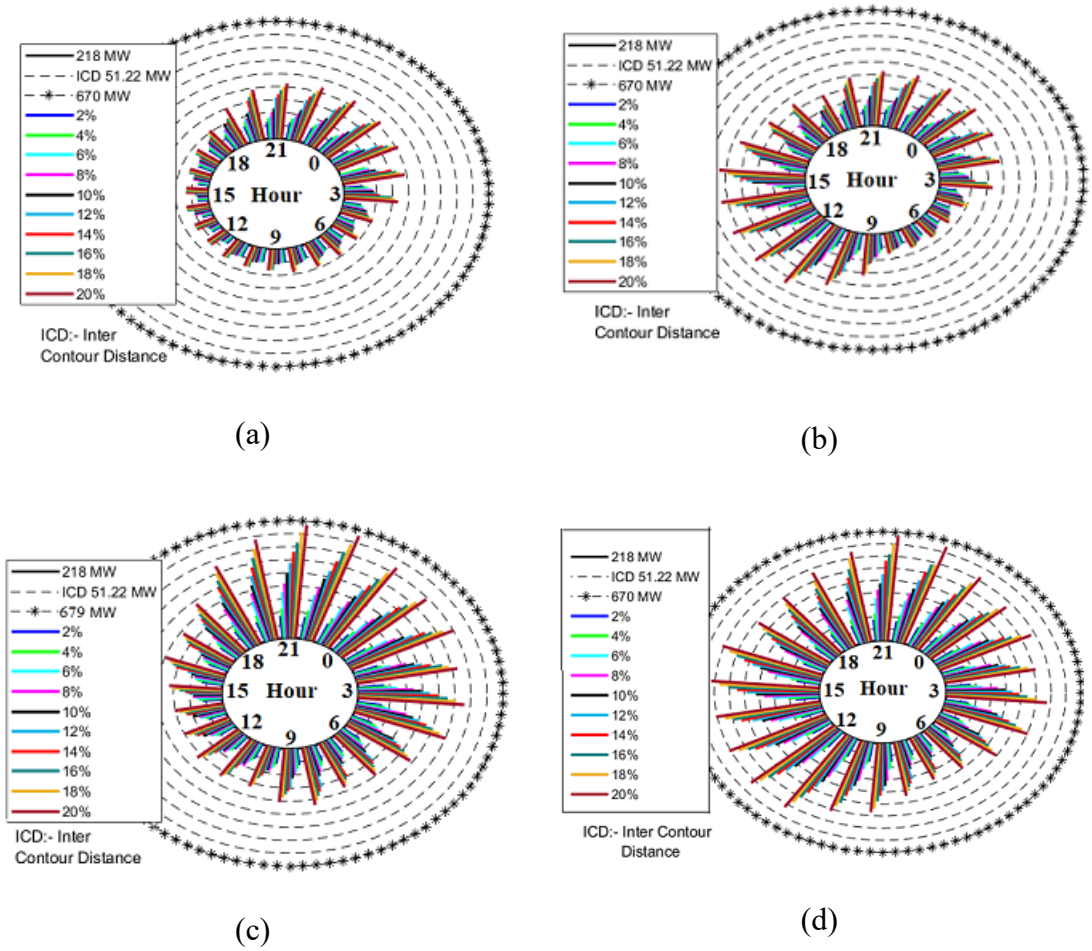

Figure 5.14 Hourly ATC (MW) for different $\%ADN_{load}$ of different cases without considering the effect of CVR (a) Hourly ATC (MW) for different $\%ADN_{load}$ without DER, (b) Hourly ATC (MW) for different $\%ADN_{load}$ with PV DER, (c) Hourly ATC (MW) for different $\%ADN_{load}$ WIND DER (d) Hourly ATC (MW) for different $\%ADN_{load}$ with PV & WIND DER

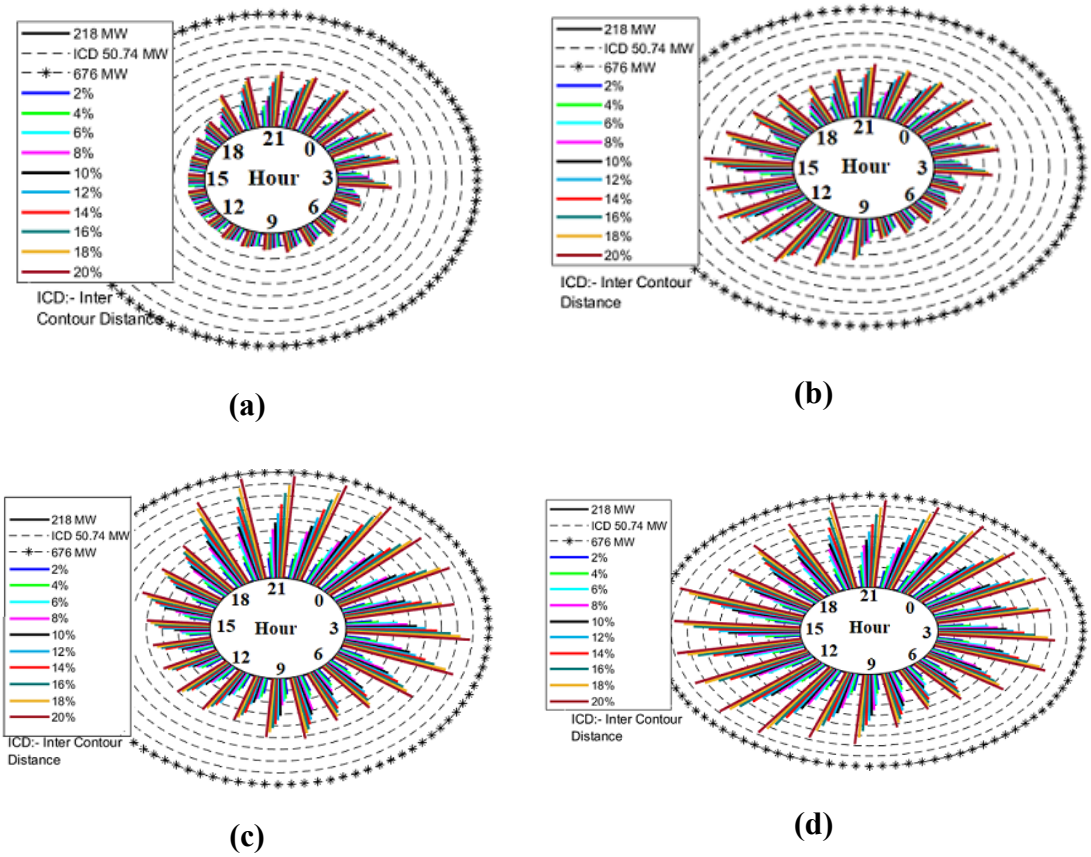

Figure 5.15 Hourly ATC (MW) for different %ADN_{load} of different cases considering the effect of CVR (a) Hourly ATC (MW) for different %ADN_{load} without DER, (b) Hourly ATC (MW) for different %ADN_{load} with PV DER, (c) Hourly ATC (MW) for different %ADN_{load} WIND DER, (d) Hourly ATC (MW) for different %ADN_{load} with PV & WIND DER

The ATC has been evaluated at ten different %ADN_{load} considering the combinations of presence/absence of the DER along with the consideration of deployment CVR at the ADN level. It can be observed that the mean value of ATC for 24 h duration increases with an increase in the %ADN_{load}. Further, the presence of DER PV, DER WIND, and DER PV& WIND increase the ATC of the system. The maximum ATC value for all the %ADN_{load} obtained when CVR is deployed is smaller than obtained without CVR. Hourly ATC (MW) for different %ADN_{load} under different cases without considering the effect of CVR has been given in Figure 5.14, whereas Figure 5.15

gives the result for the same case while considering the CVR at ADN. The figures show the ATC values (colored bars) at different hours for various $\%ADN_{load}$ plotted on 24 h clock with a circumference of the clock acting as the time axis and contours of different radius providing a reference for ATC values. It can be observed from the figures that the ATC of the system (for transaction from A1 to A2) increase with the increase in $\%ADN_{load}$. Further, the ATC values in Figure 5.14(a) and Figure 5.15(a) are higher during the night hours due to lower loads (owing to load demand profile of ADN) and lower during the day time. The ATC values during the day time increase when only PV DER is incorporated into the ADN system Figs. Figure 5.14.b and Figure 5.15.b. Overall increment in the ATC values for the whole day is observed when only WIND DER is incorporated into the ADN system, which can be easily visualized in Figure 5.14(c) and Figure 5.15(c) As the wind speed is comparatively higher during night hours, the increase in ATC during night hours is dominant than that during the day hours. Now, when both PV and WIND DER is considered, then the ATC of the system increases at all the hours of the day, which can be seen from Figure 5.14(d) and Figure 5.15(d).

5.8 CONCLUSION

In the present investigation, a co-simulation-based ITD framework has been developed to carry out different operational activities at DN, such as Volt/VAR optimization, and assess its impact on TN. The MAS driven methodology has been employed to develop the ITD framework. The optimization problem at the T&D level, as well as the combined ITD platform, has been solved using a pattern search algorithm. A case study whereby CVR has been deployed at DN, and its impact on ATC at TN have been studied. The outcomes of simulation results show that significant energy savings have been achieved

through CVR in ADN, especially during peak hours. As a result, the power is drawn from TN also reduces. The impact of reduced power demand (saved power from CVR) on ATC has been studied. Observations reveal that the ATC for transaction from source to sink area increases substantially with higher integration of DERs, and at the same time, CVR also influences the ATC. Based on the study carried out, it can be concluded that there appears a positive co-relation between ATC and CVR.